ELSEVIER

Thin Solid Films 258 (1995) 252–259

thin solid films

Oxidation behaviour of Cu–Ni(Mn) (constantan) films

W. Brückner[a], S. Baunack[a], G. Reiss[a], G. Leitner[b], Th. Knuth[c]

[a]*Institute of Solid State and Materials Research, PO Box 16, D-01171 Dresden, Germany*
[b]*Fraunhofer-Institute of Ceramic Technologies and Sintered Materials, Winterbergstraße 28, D-01277 Dresden, Germany*
[c]*microtech GmbH, Oderstraße 22, D-14513 Teltow, Germany*

Received 20 April 1994; accepted 6 September 1994

Abstract

The oxidation of constantan films has been investigated using Cu–Ni(Mn) single films and (Cu–Ni(Mn))–NiCr film configurations by measurements of electrical resistance and Auger electron spectra depth profiling, as well as by thermogravimetric and differential thermoanalytical studies. Oxidation starts under air and argon atmosphere between 300 and 350 °C. Under an N_2–H_2 gas mixture a passivating film formed by a double layer of manganese and chromium oxide reduces further oxidation strongly on the Cu–Ni(Mn) film with an NiCr adhesion layer. Further details of the oxidation mechanism are discussed in connection with the film recrystallization. A 60 nm NiCr covering layer protects well against oxidation.

Keywords: Alloys; Depth profiling; Electrical properties and measurements

1. Introduction

Cu–Ni alloys are known for their advantageous electrical and thermoelectrical properties. As constantan (CuNi44Mn1) they are used either for precision resistors with a low temperature coefficient of resistivity (TCR) or for thermocouples in combination with copper or iron. By alloying of Ni to Cu and further additions (e.g. manganese), the oxidation can be reduced in comparison with copper. The maximum temperature for use of the resistive wires is given as 600 °C [1, 2].

The material is used in bulk form as well as thin films [3–5]. To avoid the crucial surface oxidation of thin films and to give simultaneously a low contact resistance, an overlayer of NiCr is used in resistors [5–7]. The film adhesion on the oxidized silicon substrate is improved by an NiCr underlayer.

Although Cu–Ni(Mn) films are of great interest for applications, there have been up to now no special investigations of their oxidation behaviour. With bulk material the formation of a surface Cu-rich oxide and a duplex oxide layer $Cu_xO/Cu_2O/CuO/NiO$ was found [8, 9].

The present paper is focused on the oxidation of constantan films with and without both an NiCr overlayer and underlayer. The following questions are of interest. At which temperature does the oxide growth start? What influence has the atmosphere in this process? Which oxides form and what are their thicknesses? What improvements can be obtained by the NiCr protective layer? What influence does the underlayer have?

To investigate the oxidation, electrical resistance measurements, Auger electron spectroscopy (AES) and thermogravimetry (TG) in combination with differential thermal analysis (DTA) were used.

It is reasonable to assume that a non-conductive (or much more ohmic than Cu–Ni(Mn)) layer is formed by oxidation on the highly conductive constantan film. Using a layer model analogous to [10], the oxide thickness can be estimated by comparison of the resistance over temperature curves measured in oxidizing and non-oxidizing atmosphere.

Using AES experiments the thickness and the chemical composition of the oxide film can be obtained by depth profiling in combination with stylus depth measurements.

Thermogravimetric and differential thermoanalytic investigations provide results on the mass increase and the oxidation temperature. Unfortunately, for thin films on thick substrates the sensitivity is relatively low. Using the fact that thicker Cu–Ni(Mn) films delaminate from the substrate after deposition due to high tensile

stress, free-standing films can be obtained easily. These films are suitable for the TG and DTA investigations.

As is known for a lot of metallic films, e.g. Cu [11], CuNi as-deposited films recrystallize during heating [12]. This process may influence the oxidation by surface reconstruction. It can simply be studied by mechanical film stress over temperature measurements.

2. Experimental details

For the investigation of electrical, mechanical and structural properties three film systems have been chosen: 400 nm Cu–Ni(Mn), (60 nm NiCr)/(400 nm Cu–Ni(Mn)) and (60 nm NiCr)/(400 nm Cu–Ni(Mn))/(60 nm NiCr). The thermogravimetric and differential thermoanalytic measurements were done with a thicker film system of (60 nm NiCr)/(1000 nm Cu–Ni(Mn))/(NiCr overlayer) with overlayer thicknesses of 0, 60 and 120 nm.

The films were deposited by d.c. magnetron sputtering. The constantan melt metallurgical target of 160 mm diameter possessed a copper content of 57 at.% and an addition of 1 at.%Mn. The NiCr target of the same dimensions had a concentration of 37 at.%Ni.

A standard commercial sputtering plant (HZS-03 of Elektromat Dresden) was used under the usual conditions: starting pressure, 10^{-3} Pa; working pressure, 0.2 Pa Ar. The substrates (oxidized 3 in Si(100) wafers; oxide thickness, 1.2 μm) were not heated. The sputtering power amounted to 3.2 kW and 0.7 kW and the sputtering rates were about 80 nm min^{-1} and 20 nm min^{-1} for Cu–Ni(Mn) and NiCr respectively.

The film thicknesses were measured by Dektac stylus profiling. The individual NiCr thickness was evaluated from the power–time product and the rate determined for the NiCr deposition (0.344 nm W^{-1} s^{-1}).

The resistance measurements were carried out with a comb structure (measuring dimensions 7 mm × 1 mm) in a conventional four-terminal technique. The contact was made by tungsten springs. Using a heating plate, the TCR was determined between 27 and 127 °C. For ex situ experiments, four samples were measured repeatedly after heat treatment steps at 250, 300, 350, 400, 450 and 500 °C. The heat treatment was performed in a programmable process furnace over 1 h per step in air, argon or N_2–(5vol.%)H_2 mixture. The oxygen content of the Ar and N_2–H_2 gas was 3 vol. ppm (vpm) and 20 vpm, respectively. In situ electrical mesurements were performed in a quartz glass furnace in the given atmospheres between room temperature and about 550 °C. The heating and cooling rate was 4 K min^{-1}.

The AES investigations were carried out in a Perkin-Elmer PHI 660 Auger microprobe (operating at 10 keV and 100 nA). For sputter depth profiling, a rastered beam of argon ions (4 keV, $j_R = 25$ or 85 μA cm^{-2}) was used. The angle of ion incidence was 65° to the surface normal. The depth profiles were recorded in the $E \times N(E)$ mode. Owing to the overlap of Ni and Cu Auger LMM transitions, the weak Ni($L_{2,3}$MM) transition at 716 eV was observed, which resulted in a worse signal-to-noise ratio. The thickness of the oxide film was determined by stylus depth measurements at a sharp crater edge created along a molybdenum mask during depth profiling sputtering.

The TG and DTA studies were carried out simultaneously using the Simultanthermoanalysator STA 429 from Netzsch. The mass change and the thermal effects were measured in flowing air (3 l^{-1} h) during a continuous heating and cooling cycle with a rate of 10 K min^{-1}. The mass of the film sample was about 25 mg.

For characterization of recrystallization, temperature-dependent mechanical stress measurements were done using a Flexus FLX-2410 measuring system. This system determines the curvature of the silicon wafers by a laser beam reflection and detection by a position-sensitive cell, and calculates the mechanical stress by Stoney's equation [13] revised for biaxial stress

$$\sigma = \frac{1}{6} \frac{E_s}{1 - \nu_s} \frac{t_s^2}{t_f} \left(\frac{1}{r} - \frac{1}{r_0} \right) \quad (1)$$

$(E_s/(1 - \nu_s)$ is the biaxial modulus of the substrate, and equals 180 GPa for Si(100); t_s, and t_f are the thickness of substrate and film respectively; r and r_0 are the radius of curvature after and before deposition respectively). The experiments were done in air and in flowing argon and N_2–(5vol.%)H_2 gas mixture. The heating and cooling rate was 4 K min^{-1}.

3. Results

The total and the individual thicknesses for the three film configurations investigated are given in Table 1.

In Fig. 1 and Fig. 2 the dependences of the resistance and its TCR, respectively, on the annealing step temperature in different atmospheres are given for NiCr/(Cu–Ni(Mn)) films with and without an NiCr overlayer. The values of as-deposited sheet resistances $R_{s,0}$ are given in Table 1.

The similarity of the curves for the NiCr/(Cu–Ni(Mn))/NiCr structures shows that the oxidation plays a minor role for these films. The resistance increase shown by the non-protected films has consequently to be ascribed to the oxidation.

The film TCR (Fig. 2) depends only weakly on the oxide growth. Since oxide material possesses high negative TCR usually, this gives evidence for the formation of a nearly nonconductive layer on the conductive sheet. The small difference between the curves in Fig. 2 can be described qualitatively by the different thickness

Table 1
Total and individual film thicknesses and sheet resistances of the (Cu–Ni(Mn))/NiCr film configurations

Film configuration	$t_{tot,0}$ (nm)	$t_{Cu-Ni(Mn)}$ (nm)	$t_{NiCr,total}$ (nm)	$R_{s,0}$ (Ω/□)
Cu–Ni(Mn)	410	410	–	1.09
NiCr/(Cu–Ni(Mn))	457	399	58	1.10
NiCr/(Cu–Ni(Mn))/NiCr	516	400	116	1.06

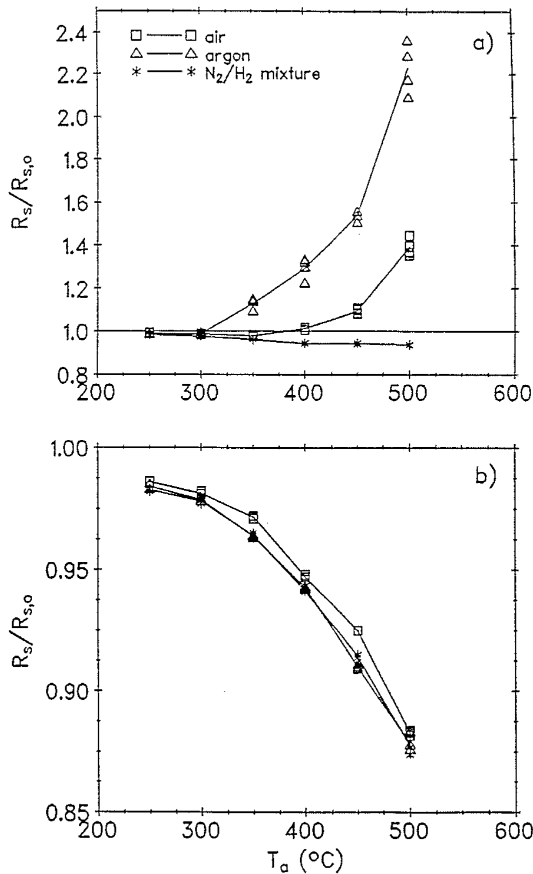

Fig. 1. Dependence of the resistance for (Cu–Ni(Mn))/NiCr films on the annealing temperature T_a under different atmospheres: (a) NiCr/(Cu–Ni(Mn)); (b) NiCr/(Cu–Ni(Mn))/NiCr.

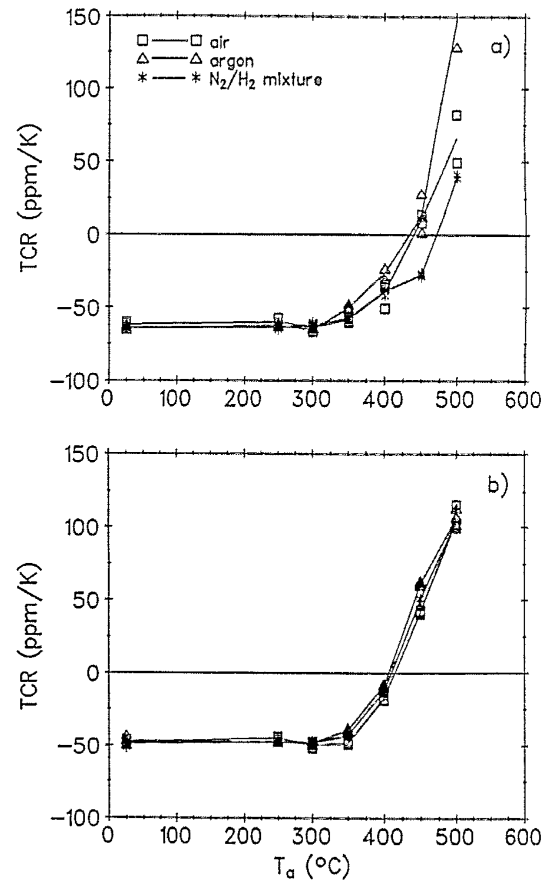

Fig. 2. Dependence of the TCR for (Cu–Ni(Mn))/NiCr films on the annealing temperature under different atmospheres: (a) NiCr/(Cu–Ni(Mn)); (b) NiCr/(Cu–Ni(Mn))/NiCr.

ratios of Cu–Ni(Mn) and NiCr according to the results in Ref. [12].

Fig. 3 shows analogous results of the continuous in situ resistance–temperature measurements during the heating and cooling cycle. For Cu–Ni(Mn) films without the protective NiCr layer the resistance is increased by oxidation above approximately 350 °C. For films with a protective NiCr layer, curves were measured as being analogous to the results in Figs. 3(a) and 3(b) for an N_2–H_2 gas mixture. Thus no clear oxidation influences could be seen.

After the stepwise heat treatment (see Fig. 1(a) and 2(a)) the films were investigated by AES. In no case could nitrogen be detected. The depth profiles of the NiCr/(Cu–Ni(Mn)) film configuration are given in Fig. 4(a) for the annealing in N_2–H_2 gas mixture. The results show the formation of a manganese oxide film immediately on the top of the film and of a chromium oxide layer under this. Both oxide layers protect the underlying Cu–Ni(Mn) against further oxidation. The situation differs from annealing in argon or air. In these cases a thick oxide layer is formed (see Fig. 4(b), as an example for oxidation in air). The oxide exhibits a two-layer structure: a Cu-rich oxide on an Ni-rich oxide. The characteristic sputter times as well as Auger linescans along the crater edge indicate that the

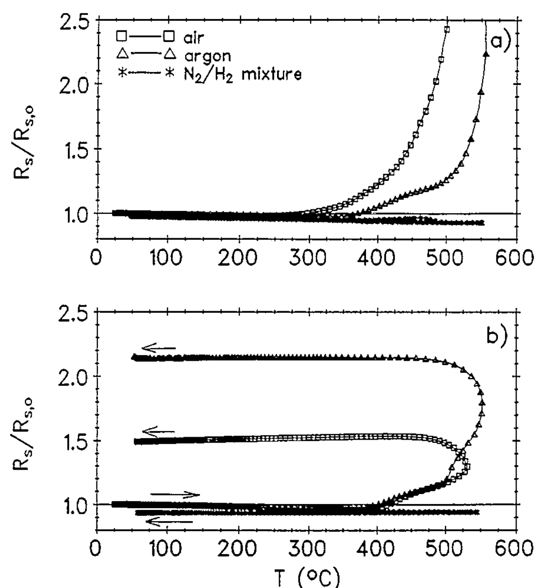

Fig. 3. Resistance change with temperature for (Cu–Ni(Mn))/NiCr films during a heating and cooling cycle under different atmospheres: (a) Cu–Ni(Mn); (b) NiCr/(Cu–Ni(Mn)).

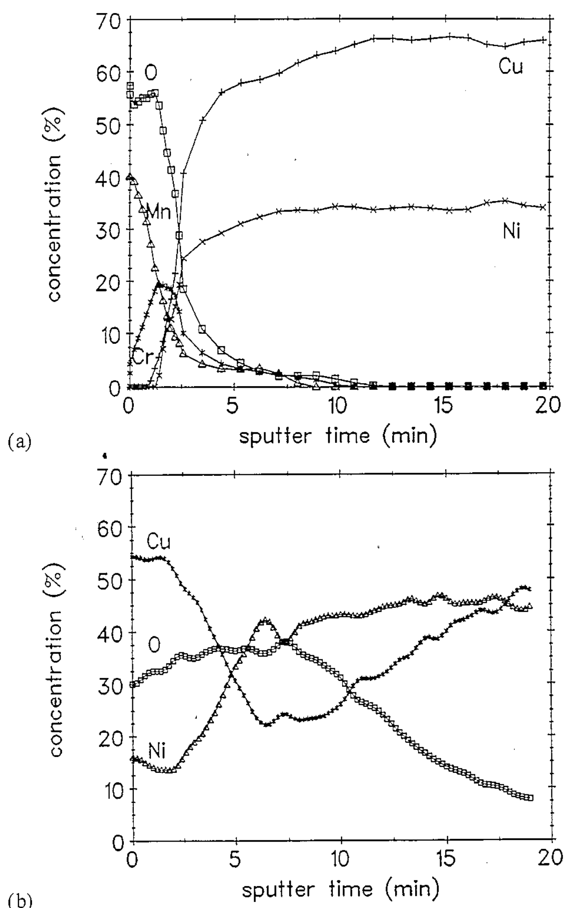

Fig. 4. AES depth profiles of the NiCr/(Cu–Ni(Mn)) film configuration after the stepwise heat treatment for the electrical measurements of Figs. 1 and 2: (a) in N_2–H_2 atmosphere ($j_r = 25$ µA cm^{-2}); (b) in air ($j_r = 85$ µA cm^{-2}).

thickness of the Cu-rich oxide is similar for oxidation both in air and in argon, whereas in the second case a thicker Ni-rich oxide layer is formed. To determine the total thickness of the oxide layer, during a special run sputtering was stopped when the oxygen signal had dropped to half of the oxide value. At the sharp crater edge produced by the shadowing mask, the total film thickness and the crater depth were measured. The results are given in Table 2 as $t_{\mathrm{tot,ox}}$ and t_{crater}. It should be noted here that the determination of the oxide thickness is affected by the rough surface of the oxide. Additionally, sputtering with argon ions induces rough crater bottoms in Cu–Ni(Mn).

In Figs. 5 and 6, results of the TG investigations on the thicker delaminated films are shown. A noticeable mass increase and, thus, oxidation starts at the marked temperatures. As indicated by the saturation, the Cu–Ni(Mn) film without the protective NiCr layer is completely oxidized during heating. Thereby the increase in mass amounts to approximately 25%. The NiCr layers protect well against oxidation. A slow mass increase shows a small oxidation of the NiCr layer. Analogous results were found on an NiCr single film too (Fig. 6). The oxidation of the protected films has a stronger effect on the TG signal than on the resistance since the resistivity ρ is higher for NiCr than for the Cu–Ni(Mn) as-deposited state: $\rho_{\mathrm{Cu-Ni(Mn)}} = 45$ µΩ cm using $\rho_{\mathrm{Cu-Ni(Mn)}} = R_{s,0} d_{\mathrm{Cu-Ni(Mn)}}$ from Table 1 and $\rho_{\mathrm{NiCr}} = 144$ µΩ cm [12]. Thus the thin NiCr layer contributes only little to the total conductivity of the film configuration.

In Fig. 7, the result of the DTA of the (58 nm NiCr)/(1000 mm Cu–Ni(Mn)) film without the protective NiCr layer is demonstrated. The exothermal oxidation effect reaches its maximum at about 680 °C.

In Fig. 8, stress–temperature curves for Cu–Ni(Mn) single films are drawn for different heating atmospheres. They show thermal stress components at lower temperatures with a linear $\sigma(T)$ dependence according to the relation

$$\frac{\mathrm{d}\sigma}{\mathrm{d}T} = \frac{E_f}{1 - \nu_f}(\alpha_s - \alpha_f) \tag{2}$$

($E_f/(1 - \nu_f)$ is the biaxial modulus of the film; α_s and α_f are the linear coefficient of the thermal expansion of substrate and film respectively). At high temperatures plastic stress reduction is observed. In the temperature range between 200 and 350 °C of the heating curves, tensile stress components ($\Delta\sigma > 0$) result from material densification by recrystallization. These recrystallization effects are spread over different temperature intervals for the different annealing atmospheres. Especially for heating in argon, they occur in a small temperature range (300–325 °C).

Table 2
Parameters of the partially oxidized NiCr/(Cu–Ni(Mn)) films during heat treatment in air and argon [a]

Atmosphere	$t_{tot,ox}$ (nm)	t_{crater} (nm)	$\Delta t_{Cu\text{-}Ni(Mn),th}$ (nm)	$\Delta t_{Cu\text{-}Ni(Mn),cr}$ (nm)	$\Delta t_{Cu\text{-}Ni(Mn),r}$ (nm)
Air	550	220	139	175	157
Argon	800	640	346	335	253

[a]For initial thicknesses see $t_{tot,0}$ in Table 1.

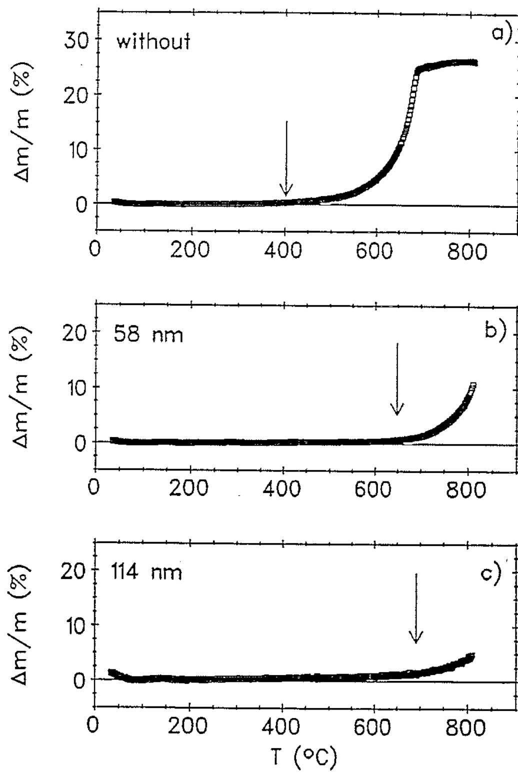

Fig. 5. Mass increase by oxygen uptake in thermogravimetric measurements on the film configurations with 58 nm NiCr underlayer and 1000 nm Cu–Ni(Mn), for different thicknesses of the protective NiCr layer.

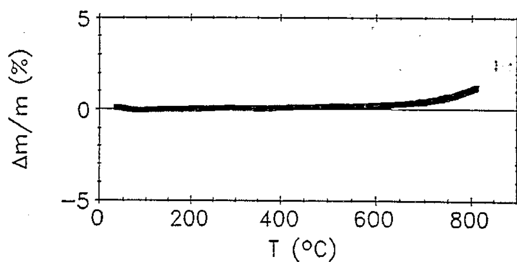

Fig. 6. Mass increase in thermogravimetric measurements on a single NiCr (thickness 3.5 μm).

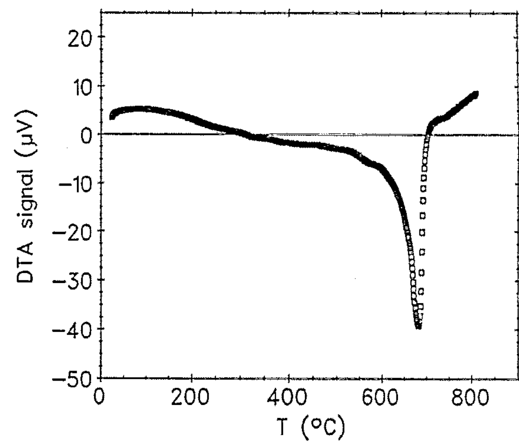

Fig. 7. DTA of a (58 nm NiCr)/(1000 nm Cu–Ni(Mn)) film configuration delaminated from the oxidized silicon wafer.

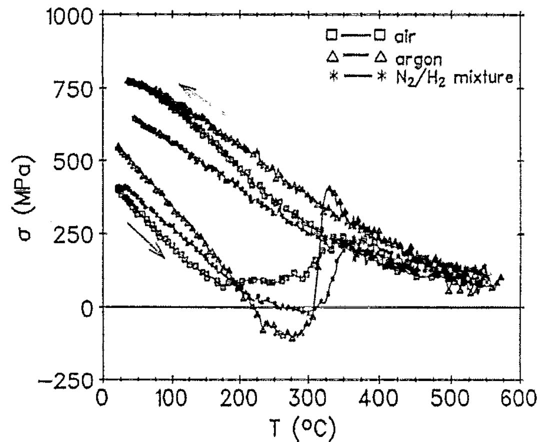

Fig. 8. Dependence of the mechanical stress of Cu–Ni(Mn) films on temperature under different atmospheres.

4. Discussion

4.1. Model

For the discussion of oxidation of NiCr/(Cu–Ni(Mn)), a layer model can be assumed (Fig. 9).

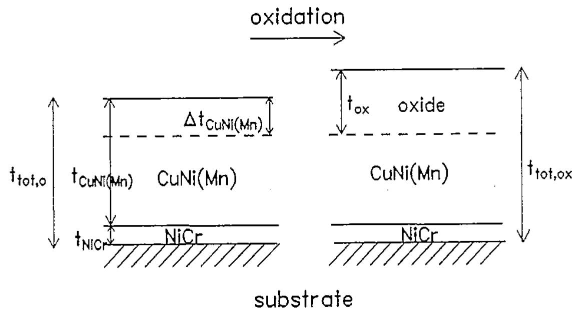

Fig. 9. Layer model.

When a portion $\Delta t_{\text{Cu-Ni(Mn)}}$ of the Cu–Ni(Mn) film is oxidized, this results in an oxide film thickness t_{ox}. The following relation is valid for the thickness ratio $t_{ox}/\Delta t_{\text{Cu-Ni(Mn)}}$ in a homogeneous oxide layer neglecting stress formation:

$$\frac{t_{ox}}{\Delta t_{\text{Cu-Ni(Mn)}}} = \frac{M_{\text{oxide}}}{M_{\text{Cu-Ni(Mn)}}} \frac{\rho_{\text{m,Cu-Ni(Mn)}}}{\rho_{\text{m,oxide}}} = \beta_{\text{Cu-Ni(Mn)}} \quad (3)$$

(t_{ox} and $\Delta t_{\text{Cu-Ni(Mn)}}$ are explained in Fig. 9, $M_{\text{Cu-Ni(Mn)}}$ and M_{oxide} are the molecular weights of Cu–Ni(Mn) and its oxide, $\rho_{\text{m,Cu-Ni(Mn)}}$ and $\rho_{\text{m,oxide}}$ are the density of Cu–Ni(Mn) and its oxide respectively). This thickness ratio is called the Pilling–Bedworth ratio β in the oxidation theory [14]. It corresponds to the ratio of the mean volume per metal ion in the oxide to the mean volume per metal atom in the alloy.

Under simplifying assumptions (dense structure, validity of the layer model, oxidation of the Cu–Ni(Mn) only) the following relations between the thickness of the oxidized film and the total film thickness t_{total}, the final mass m_{total} and the sheet resistance $R_{\text{s,total}}$ of the NiCr/(Cu–Ni(Mn)) configuration can be deduced:

$$t_{\text{total}} = t_{\text{tot,0}} + t_{ox}(\beta_{\text{Cu-Ni(Mn)}} - 1) \quad (4)$$

$$m_{\text{total}} = m_{\text{tot,0}} + t_{ox}\beta_{\text{Cu-Ni(Mn)}}\rho_{\text{m,oxide}} \quad (5)$$

$$\frac{1}{R_{\text{s,total}}} = \frac{1}{R_{\text{s,0}}} - \frac{t_{ox}}{\rho_{\text{Cu-Ni(Mn)}}} \quad (6)$$

(for the symbols, see Fig. 9; the index 0 denotes the initial (unoxidized) case; $\rho_{\text{Cu-Ni(Mn)}}$ is the resistivity of Cu–Ni(Mn)).

In the first term these equations contain the properties of the oxide-free film, e.g. structural reconstructions and interdiffusion [12]. The behaviour of a protected Cu–Ni(Mn) film which is nearly oxidation resistant can be considered as that of the oxide-free NiCr/(Cu–Ni(Mn)) film.

The ansatz of dividing the Cu–Ni(Mn) film into a non-conductive oxide and a conductive part is reasonable, since the TCR of the conductive part corresponds to the behaviour of a (Cu–Ni(Mn))/NiCr double layer. Thus the TCR is not shifted by the growth of an oxide layer. Similar results have already been found for CrSi films [10].

4.2. *Pilling–Bedworth ratio*

The formation of oxide Cu^{2+} and Ni^{2+} is assumed. Neglecting the Mn addition, with complete oxidation of the Cu–Ni(Mn) layer in the NiCr/(Cu–Ni(Mn)) film configuration without an NiCr protective layer, a mass increase of 22.7% can be expected. This increase amounts to 24.7% if the NiCr underlayer is oxidized too. The results of Fig. 5(a) ($\Delta m/m = 25\%$ during oxidation) confirm the assumption of formation of a divalent oxidation state of Cu and Ni. Nevertheless, in the initial stage of oxidation Cu_2O may be formed, being typical for copper and having passivating properties.

Assuming the full oxidation of Cu–Ni(Mn), a Pilling–Bedworth ratio $\beta_{\text{Cu-Ni(Mn)}} = 1.63$ can be estimated by Eq. (3). As densities $\rho_{\text{m,CuO}} = 6.42$ g cm^{-3} and $\rho_{\text{m,NiO}} = 7.45$ g cm^{-3} [15] were used.

4.3. *Oxide film thicknesses*

Especially according to the electrical measurements, the oxidation of Cu–Ni(Mn) depends strongly on the atmosphere. In the N_2–H_2 gas mixture the oxidation of Cu–Ni(Mn) is low up to 500 °C. In argon the oxide growth starts at about 300 °C and in air a little below 350 °C. For shorter treatments (e.g. during the heating ramp with 4 K min^{-1}) these temperatures are higher by about 50 K.

It is surprising that the annealing in argon leads to the formation of a thicker oxide layer than in air. The reason will be discussed below.

With the NiCr/(Cu–Ni(Mn)) samples after the stepwise heat treatment in different atmospheres for the electrical mesurements, the thicknesses of the oxidized Cu–Ni(Mn) layer need to be evaluated. This was done (Table 2) (a) from the sputtering crater depth t_{crater} by

$$\Delta t_{\text{Cu-Ni(Mn),cr}} = t_{\text{tot,0}} - t_{\text{crater}} \quad (7)$$

(b) from the increase of total thickness during oxidation $t_{\text{tot,ox}}$ by

$$\Delta t_{\text{Cu-Ni(Mn),th}} = (t_{\text{tot,ox}} - t_{\text{tot,0}})/\beta_{\text{Cu-Ni(Mn)}} \quad (8)$$

and (c) from the resistance change during the heat treatment procedure by Eq. (6). For the evaluation it was simplifyingly assumed that the sheet resistance of the NiCr/(Cu–Ni(Mn)) films in the unoxidized case $R_{\text{s,0}}$ is equal the sheet resistance of the NiCr/(Cu–Ni(Mn))/NiCr film configuration (compare Table 1) and that the change of resistivity of Cu–Ni(Mn) with annealing corresponds to the sheet resistance decrease of this configuration in Fig. 1(b).

The agreement of the thicknesses of the oxidized Cu–Ni(Mn) films in Table 2 is very good with the exception of $\Delta t_{Cu\text{-}Ni(Mn),r}$ for argon. However, in this case with a thin remaining unoxidized Cu–Ni(Mn) film, inhomogeneities (e.g., roughness of the oxide–metal interface) become important for the electrical transport behaviour.

4.4. Oxide layer analysis

During the heat tretment of NiCr/(Cu–Ni(Mn)) films in the N_2–H_2 gas mixture, a surface manganese oxide and chromium oxide double layer forms, hindering further oxidation. Manganese and chromium can reach the surface only by diffusion. The Cr comes from the adhesion layer and contributes to the improvement of the oxidation resistance. The formation of a protective Cr_2O_3 layer is also known from CuCr thin films [16].

Obviously, the transport of manganese and chromium does not occur during annealing in argon and in air. Thus, the protecting manganese oxide/ chromium oxide double layer is not formed. The beneficial effect of the hydrogen lies in the fact that in the reducing gas only the most stable oxides (formation enthalpies: Mn_3O_4, 1386 kJ mol^{-1}; Cr_2O_3, 1141 kJ mol^{-1}; MnO, 384 kJ mol^{-1}; NiO, 240 kJ mol^{-1}; Cu_2O, 170 kJ mol^{-1}; CuO, 165 kJ mol^{-1} [17]) can survive. Additionally, interaction with hydrogen may promote the diffusion within the layer.

As a result of the interaction with air and argon, an oxide double layer is formed. This is in agreement with results on bulk Cu–Ni [9]. Owing to the roughness of the oxide it was impossible to decide whether the layer is composed of alternating copper oxide and nickel oxide or mixtures of both oxides with composition changing with depth. The phase diagram of Cu–Ni–O does not show formation of new oxides, but CuO is soluble in NiO [18]. NiO is known to be a good passivating layer whereas the near-noble metal Cu forms bad passivating layers. Thus the nickel oxide or nickel-rich oxide is assumed to be the rate-limiting barrier in oxide growth. Owing to lack of oxygen during annealing in Ar, a worse and therefore thicker oxide is formed. The partial pressure of oxygen in argon was in the order of 10^{-2} Pa.

4.5. Influence of recrystallization

The stress increase between 200 and 350 °C is caused by recrystallization. The grain growth was also shown by former transmission electron microscopy studies [12]. Influenced by the heat treatment atmosphere (and grain boundary diffusion), the recrystallization during the heating ramp especially in argon happens quickly in a small temperature interval between 300 and 325 °C. During this interval the stress changes from a compressive to a tensile one. Indicated by a steep dropping off of the intensity of the reflected laser beam of the stress-measuring system, the surface roughens by grain growth. It is speculated that, by the sharp stress transition and rebuilding of the surface, an existing thin protective layer will be destroyed and a very reactive new surface will be formed. Therefore the oxidation in argon starts rapidly after the recrystallization.

4.6. Influence of the NiCr protection

All the electrical measurements as well as the TG studies show that the NiCr protects well against oxidation. Already with a film thickness of 60 nm, the temperature of the beginning of Cu–Ni(Mn) oxide growth is increased by about 200 K. According to TG studies (Figs. 5 and 6), the oxidation of NiCr proceeds slowly. Results in the literature [19, 20] show that highly passivating Cr_1O_3 forms on the top of the NiCr films.

5. Conclusions

Although in comparison with copper the oxidation resistance of Cu–Ni(Mn) alloys is improved by the addition of Ni and Mn, the oxidation of constantan films remains a serious and interesting question.

The following conclusions can be drawn from the discussed results.

(1) During annealing in air or argon atmosphere for about 1 h, the oxidation of Cu–Ni(Mn) starts at about 300–350 °C. The oxide growth was stronger in Ar (with about 3 vpm oxygen) than in air. In both annealing atmospheres a (Cu–O)/(Ni–O) oxidic double layer forms.

(2) When the heat treatment was done in an N_2–H_2 gas mixture, the oxidation of Cu–Ni(Mn) with NiCr underlayer (adhesion film) is reduced strongly. Thereby a surfacial protecting Mn–O and Cr–O double layer forms. This process requires the diffusion of Mn and Cr to the surface.

(3) Strong recrystallization and surfacial reconstruction demonstrated in the $\sigma(T)$ curves were discussed as being the cause of the start of strong oxidation in an argon atmosphere.

(4) In the final state, the Cu–Ni(Mn) film oxidizes into the divalent state of the metal ions (CuO,NiO or mixed oxide).

(5) A covering NiCr layer with a thickness of about 60 nm hinders the oxidation effectively.

(6) Cu–Ni(Mn) is an interesting resistive thin film material, but it forms a "self-passivating" oxide surface layer only during annealing in the N_2–H_2 gas mixture. This is a disadvantage compared with CrSi [21], NiCr[20] or CuCr [16].

Acknowledgements

The authors are indebted to Professor A. Heinrich for helpful activities and discussions. This work was supported in part by the Bundesministerium für Forschung und Technologie of the FRG under Contract 03 M 3040 7.

References

[1] W. Bergmann, *Werkstofftechnik*, Vol. 1, Hanser, Munich, 1989, p. 246; Vol. 2, p. 511.
[2] F. Kohlrausch, *Praktische Physik*, Vol. 3, Teubner, Stuttgart, 1968, p. 84.
[3] I. Nishino, Y. Ichinose, Y. Sorimachi and I. Tsubata, *Int. J. Hybrid Microelectron., 6* (1985) 18.
[4] D. Elefant, A. Heinrich and J. Schumann, *Proc. 10th Tagung Hochvakuum, Grenzflächen/Dünne Schichten, Dresden, 19–21 March, 1990*, Vol. 1, Physikalische Gesellschaft der DDR, Berlin 1990, p. 111.
[5] W. Brückner, J. Schumann and H. Grießmann, *Phys. Status Solidi A, 140* (1993) K21.
[6] J. Schumann, D. Elefant and A. Heinrich, *Tagung Wer macht was in den physikalischen Technologien, Berlin, 11–13 June 1990*, Vol. Poster I, VDI-Technologiezentrum Physikalische Technologien, Düsseldorf, 1990, p. 221.
[7] W. Hinüber, J. Schumann, D. Elefant and W. Jarzak, *Proc. ELMAT 91, Essen, 22–24 January 1991*, vde-Verlag GmbH Berlin und Offenbach, 1991, p. 181.
[8] K. Tsuji and K. Hirokawa, *Surf. Interface Anal., 17* (1991) 819.
[9] R. Souchet, M. Lenglet, P. Miche, S. Weber and S. Scherrer, *Analusis, 21* (1993) 173.
[10] H. Grießmann, W. Brückner and H. Schreiber, *Thin Solid Films, 226* (1993) 110.
[11] P. A. Flinn, *J. Mater. Res., 6* (1991) 1498.
[12] W. Brückner, J. Schumann, S. Baunack, W. Pitschke and Th. Knuth, *Thin Solid Films, 258* (1995) 236.
[13] G. G. Stoney, *Proc. R. Soc. London, Ser. A, 82* (1909) 172.
[14] M. Schütze, *Die Korrosionsschutzwirkung oxidischer Deckschichten unter thermisch-chemisch-mechanischer Werkstoffbeanspruchung*, Gebrüder Borntraeger, Berlin, 1991, p. 19.
[15] G. V. Samsonova, *Fiziko-chimiceskije svojstva okislov*, Metallurgija, Moscow, 1978, p. 29.
[16] J. Schumann, W. Brückner and A. Heinrich, *Thin Solid Films, 228* (1993) 44.
[17] H. Landolt and R. Börnstein, *Zahlenwerte und Funktionen*, Vol. 2, Springer, Berlin, 1961, Part 4, p. 179 ff.
[18] N. G. Schmahl and F. Mueller, *Z. Anorg. Allg. Chem., 332* (1964) 217.
[19] H.-J. Anklam, *Thin Solid Films, 121* (1984) 61.
[20] I. E. Klein, M. Hershkovich and I. A. Goldberg, *Microelectron. J., 19* (1989) 17.
[21] W. Brückner, H. Grießmann, H. Schreiber, H. Vinzelberg and A. Heinrich, *Thin Solid Films, 214* (1992) 84.